sustainability

MDPI

Article

Error Influence Simulation of the 500 m Aperture Spherical Radio Telescope Cable-Net Structure Based on Random Combinations

Lulu Wang [1], Mingmin Ding [1,*], Yangjie Ruan [2], Bin Luo [2] and Jianchen Guo [1]

[1] College of Civil Engineering, Nanjing Forestry University, Nanjing 210037, China
[2] National Prestress Engineering Research Center, Key Laboratory of C & PC Structures of Ministry of Education Southeast University, Nanjing 210096, China; seurobin@seu.edu.cn (B.L.)
* Correspondence: dmm1989@njfu.edu.cn

Abstract: The reflector of a Chinese 500 m aperture spherical radio telescope is supported by a giant cable-net structure. In the actual operation process, active displacement observation is realized by connecting the actuators with the control cables to adjust the cable net, which requires high manufacturing and installation accuracy. In this study, an error sensitivity computing method based on a normal distribution is adopted to perform single-error computing and multi-error coupling computing and to investigate the effect of the length error of all the cables, tensioning force error of active surface cables, and installation error of external nodes on the cable force. The results show that the length error of the surface cables and the installation error of the external nodes are the main factors affecting the cable force, while the length error of the control cables is a secondary factor. The coupling effect of multiple errors is not the linear superposition of each error's influence; therefore, all the error factors should be comprehensively considered for coupling computing to determine the control index. Through multi-error coupling computing, it is determined that the length error limits of the surface cables and control cables are ±1.5 mm and ±20 mm, respectively, the tensioning force error limit of the active surface cables is ±10%, and the installation error limit of the external nodes is ±50 mm.

Keywords: giant cable-net structure; error influence computing; single-error computing; multi-error coupling computing

Citation: Wang, L.; Ding, M.; Ruan, Y.; Luo, B.; Guo, J. Error Influence Simulation of the 500 m Aperture Spherical Radio Telescope Cable-Net Structure Based on Random Combinations. *Sustainability* **2023**, *15*, 15061. https://doi.org/10.3390/su152015061

Academic Editors: Pedro Muñoz-Velasco and Viviana C. Letelier Gonzalez

Received: 29 July 2023
Revised: 26 September 2023
Accepted: 17 October 2023
Published: 19 October 2023

1. Introduction

Unlike traditional structures [1,2], the 500 m aperture spherical radio telescope is the world's largest single-aperture radio telescope [3–5]. Active deformation is the most obvious characteristic of the telescope's reflector. Through active control, a 300 m aperture instantaneous paraboloid is formed in the observation direction to converge electromagnetic waves (Figure 1). During observation, the paraboloid moves on the 500 m aperture spherical crown with the movement of the observed celestial body to realize tracking observation. When the telescope is working, the reflecting surface should change its surface shape in real time as needed to simulate a desired parabolic surface. To achieve this goal, the reflective surface is divided into 1788 spherical hexagonal basic units [6], each of which has a spherical hexagonal shape with a length of no more than 7.5 m on one side. The reflective panel is a grid panel supported on a hexagonal support structure, as shown in Figure 2.

The supporting structure of the active reflective surface is a hemispherical cable-net structure, as shown in Figure 3, which consists of 6670 surface cables, 2225 connecting nodes, 2225 control cables, and 1 steel ring truss [6,7]. Based on the shape of the triangular grid elements, the surface cables are woven into a spherical cable net to lay the reflective panel [8,9]. The supporting structure around the reflecting surface includes a steel ring beam and steel lattice column [10]. The cable-net structure is fixed on the steel ring beam through 150 edge surface cables [11]. These 150 edge surface cables are external cables, also called active surface cables, which can be adjusted in length and tension.

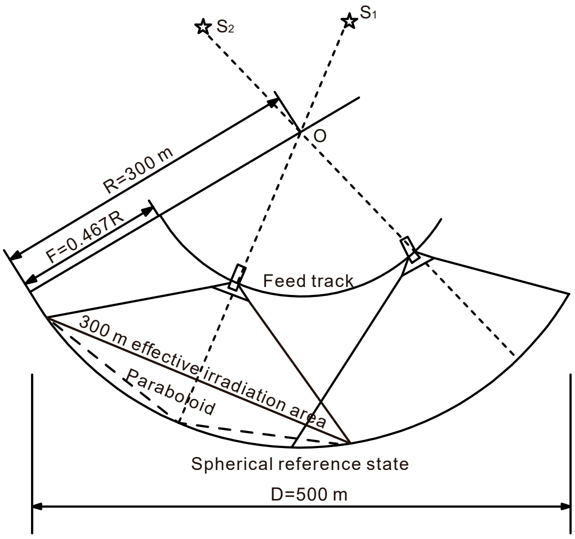

Figure 1. Working principle of active deformation for the 500 m aperture spherical radio telescope. (S_1 and S_2 represent the possible orientations of the target observation object.)

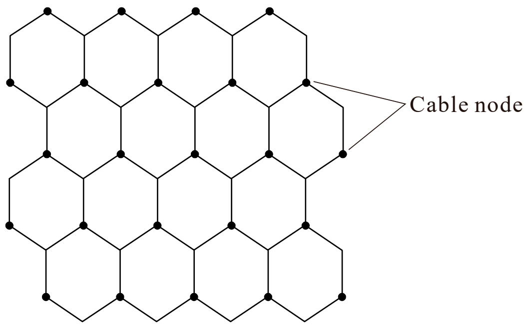

Figure 2. Relationship between the basic units of the reflecting surface and arrangement of actuators.

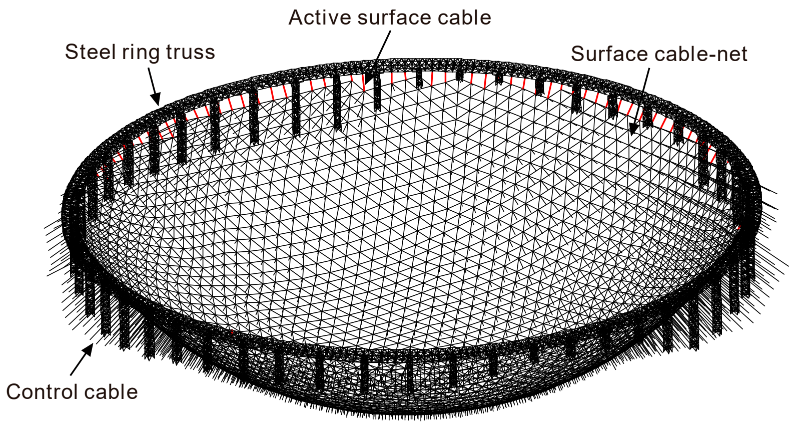

Figure 3. Schematic diagram of the 500 m cable-net structure.

The external cables are connected to the surrounding supporting structures through external nodes. The surface cables are connected to control cables at the cable nodes, and the deformation of the cable net is controlled by adjusting the length of the actuator to realize the active displacement of the reflecting surface from the spherical surface to the paraboloid, which is displayed in Figure 4.

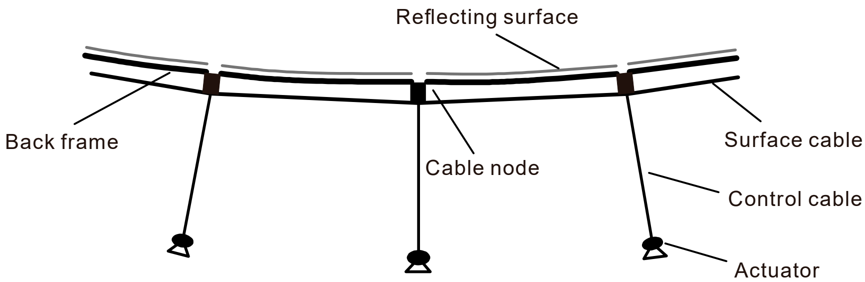

Figure 4. Schematic diagram of the active reflector of the 500 m aperture spherical radio telescope.

In contrast to composite structures [12,13] or new structures [14], the design of cable-stiffened latticed shells [15] and Tensairity domes [16] or trusses [17,18] is a definite process, while the errors in the fabrication and installation processes of cable nets are random. The lengths and elastic moduli of all the cables, the coordinates of the boundary nodes, the coordinates of the control cable actuators, and the tensioning forces of the active surface cables will produce errors. These errors couple and generate considerable randomness, which will affect the final forming accuracy of the cable net. In actuality, a minuscule error may lead to unsatisfactory fitting accuracy between the cable net and the active paraboloid and will affect the safe operation and observation accuracy of the entire structure, especially for a 500 m diameter giant cable-net structure. In this case, error influence computing is needed to find the acceptable error limit for each parameter, which is uncertainty quantification [19,20].

Commonly used parameter computing methods can be divided into single-error influence methods and multi-error coupling influence methods. Single-error influence computing only tests the impact of single-parameter variation on the model results, and the other parameters remain unchanged. In contrast, multi-error coupling influence analysis tests the impact of the variations in multiple parameters on the model results and analyzes the impacts of each parameter and the interaction between parameters on the model results.

Bonizzoni et al. [21,22] adopted a perturbation approach by developing an algorithm for solving the recursive first-moment problem approximately in the tensor-train format and proved that well-posedness and regularity results for the recursion were able to hold in Sobolev space-valued Holder spaces with mixed regularity. This method could also be applied to error sensitivity computing of cable-supported structures. Chen et al. [23] set up a mathematical model of element length error for cable-bar tensile structures based on probability statistics theory and indicated that the construction scheme has a great impact on cable errors. Zong et al. [24] proposed an analytical error influence computing method of the shape precision for antenna structures and found that slender cables and high tension levels can improve the overall structural ability to resist the effects of uncertainties on antenna performance. Luo et al. [25] pointed out that the lengths of passive cables, the tensioning forces of active surface cables, and the installation coordinates of external nodes are the main factors affecting the forming state of cable-strut tensile structures. They proposed the 'small elastic modulus' method to analyze the random error combinations of cable length and tensioning force and then determined the control index of practical engineering. Chen et al. [26] carried out an optimization of the construction scheme of a cable-strut tensile structure based on error sensitivity computing and found that different elements had different error sensitivities. By replacing certain bars of the shell with passive viscoelastic dampers and by applying the eigenvalue perturbation technique and the earthquake spectrum concept, Chen et al. [27] formulated an element length error model for cable-strut tensile structures, derived the fundamental equation of pre-tension deviation and element length error, and found that cables are more sensitive to errors than struts. Yang [28] analyzed the sensitivities of various topologies of the reticulated shell. Sun et al. [29] mathematically deducted the sensitivity of reflector surface accuracy with respect to the random errors of the unstressed cable length and proposed a nonbutton connecting method. Jin et al. [30] proposed a global error influence computing method and concluded that the lengths of the cables and the size of the cable cross-sectional area are important factors influencing the cable net of a 500 m aperture spherical radio telescope. Xu et al. [31] performed a detailed parameter analysis for a 500 m aperture spherical radio telescope and found that the blanking length deviation of cables is the most important factor influencing the cable force, while the deviation of the edge cable nodes and the friction coefficient of the sliding support mainly affect the variation in the cable forces of the 150 surface cables of the outermost ring. Since the outermost 150 surface cables are actively tensioned cables, the tensioning forces of these active surface cables can be directly regarded as one of the main factors influencing errors. Figure 5 illustrates the section diagram of the active reflector.

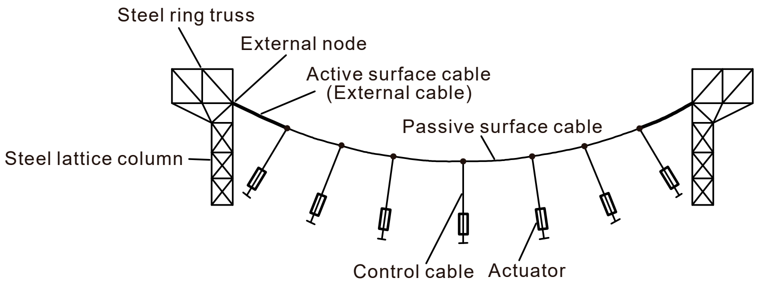

Figure 5. Section diagram of the active reflector of the 500 m aperture spherical radio telescope.

The source of errors has also been discussed in other studies, and the structural response in actual engineering could be obtained by recent references. An interval uncertainty-oriented optimal control method based on the linear quadratic regulator (LQR) [32] was proposed to balance both minimizations of the optimal control cost function and state vector fluctuation for spacecraft attitude control. An interval dynamic model [33] of a space power satellite (SPS) was presented based on a nonprobabilistic theory to consider multisource uncertainties and disturbances in attitude dynamics. An uncertain optimal attitude–vibration control method for rigid–flexible coupling satellites with reliability constraints [34] was proposed based on interval dimension-wise analysis. A novel placement and size-oriented heat dissipation optimization [35] was proposed for a space solar power satellite based on an interval dimension-wise method considering both design and uncertain variables to balance the mass and temperature distribution in the antenna module. A sensor placement algorithm for structural health monitoring based on an iterative updating process [36] was proposed and applied to different structures owing to the use of adaptive weight factors in the combined objective. A time-dependent, reliability-based method for optimal load-dependent sensor placement [37] was proposed by using nonprobabilistic theory to characterize the uncertainty in the propagation process for model updating. Based on the unbiased estimate of modal coordinates with a reduced and full model in the deterministic case, Yang et al. [38] treated uncertainties as interval numbers, and the propagation of uncertain modal coordinates was presented based on nonprobabilistic theory.

As stated above, the main factors influencing the errors of a giant cable-net structure are the cross-sectional areas of the cables, the lengths of the surface cables and control cables, the tensioning forces of the active surface cables, and the installation coordinates of the external nodes. Existing studies have discussed the influence of element length, stress level, member type, cable position, and other factors on the overall error of cable-net structures, which gives context for this work. In some of these studies, the influence of individual errors on the giant cable net was analyzed. However, single-error influence computing and multi-error coupling influence analysis of the overall structure have not been considered simultaneously, especially when the cross-sectional area of each cable is determined in advance after design. To explore the error sensitivity, find the main error control index, and provide specific parameters for the pre-evaluation and health monitoring system of the FAST cable-net structure [39], this study takes the lengths of the surface cables and control cables, the tensioning forces of the active surface cables, and the installation coordinates of the external nodes as the parameter variables; uses single-error and multi-error methods to analyze the error influence; compares the influence of various errors on the prestress level of the cable net; and determines a reasonable construction accuracy control index.

2. Error Influence Computing Method

The Monte Carlo method [40] (i.e., random sampling method) belongs to a branch of experimental mathematics. This method uses random numbers to carry out statistical experiments and takes the obtained statistical moments (e.g., mean value, probability) as the numerical solution of the problem to be solved. The detailed computing steps of the Monte Carlo method are listed as follows:

(1) Build the error model, which is the basis of analyzing random error.
(2) Determine the probability distribution of the corresponding structural error according to the characteristics of the error source and its influence on the structural error.
(3) Randomly generate a group of structural error combinations and substitute them into the error model to calculate the structural internal force errors according to the probability distribution determined in step (2).
(4) Repeat the above process n times to obtain n error values. If n is large enough, the distribution of error values tends to the real probability distribution. Therefore, these error values can be used to describe the probability characteristics of the real error.

2.1. Selection of Single Random Error

In this study, the system error of cable length, installation coordinate error of external nodes, and tensioning force error ratio of active surface cables were selected as the parameter variables. Among them, the system error of cable length can be abbreviated as cable length error, which consists of the fabrication error of cable length, measurement error of cable length, and fabrication error of pin holes. The installation error of external nodes is mainly determined by the characteristics of surrounding support structures and the form of external connecting nodes. The tensioning force error ratio of active surface cables is mainly determined by the tensioning equipment and tensioning method.

Table 1 lists the allowable ranges of cable length error in the Chinese specification (JGJ 257-2012) [41] and the American ASCE specification (ASCE/SEI STANDARD 19-10) [42]. The requirements of the American specification are more stringent than those of the Chinese specification. Furthermore, according to the Chinese specification, the allowable error limit of the tensioning force of the cable-net structure is ±10%, which is not specified in the ASCE specification.

Table 1. Error limits of cable length specified in Chinese and American specifications.

Standard	Total Cable Length L_0 (m)	Error Limit ΔL (mm)
Chinese specification (JGJ 257-2012) [41]	≤ 50	± 15
	$50 < L_0 \leq 100$	± 20
	>100	$L_0/5000$
American specification (ASCE/SEI STANDARD 19-10) [42]	≤ 8.54	± 2.54
	$8.54 < L_0 \leq 36.59$	$\pm 0.03\%\ L_0$
	>36.59	$\pm(\sqrt{L_0}+5)$

The actual cable length, the actual coordinates of the external node, and the actual tensioning force of an active surface cable can be expressed as

$$\begin{cases} L = L_0 + \Delta_L \\ C = C_0 + \Delta_C \\ T = (1 + \Delta_T)T_0 \end{cases} \tag{1}$$

where L is the actual cable length, C is the actual coordinate of the external node, T is the actual tensioning force of the external cable, L_0 is the designed cable length, C_0 is the designed coordinate of the external node, T_0 is the designed tensioning force of the external cable, Δ_L is the cable length error, Δ_C is the installation error of the external node, and Δ_T is the tensioning force error of the external cable.

According to the central limit theorem of Lindbergh and Levy, e.g., X~N (m, s^2), if each influencing factor is independent and the possibility of positive deviation or negative deviation caused by each factor is the same, it can be considered that the cable length error X approximately obeys a normal distribution. The distribution function of the cable length error is

$$f(x) = \frac{1}{\sqrt{2\pi}\sigma}\exp\left(-\frac{(x-\mu)^2}{2\sigma^2}\right) \tag{2}$$

where μ is the mean value of the cable length error and σ^2 is the variance of the cable length error.

Assume that the allowable range of the component's fabrication and installation is [$X_{\min}$, $X_{\max}$] and $P(X_{\min} < X < X_{\max})$ = 95%, in which $X_{\min}$ and $X_{\max}$ are the lower limiting value and upper limiting value of the cable length error, respectively. The value of μ and the approximate value of σ can be calculated as

$$\mu = \frac{X_{\max} + X_{\min}}{2} \tag{3}$$

$$\sigma \approx \frac{X_{\max} - X_{\min}}{4} \tag{4}$$

2.2. Multiple Random Error Combinations

The giant cable-net structure is fixed on the steel ring beam through 150 active surface cables. The installation coordinate error of an external cable node is equivalent to the additional length error of an external cable. Therefore, the total cable length error of an external cable can be defined as:

$$\delta^a_{lc(i,j)} = \delta^a_{l(i,j)} + \delta^a_{c(i,j)} \tag{5}$$

where $\delta^a_{lc(i,j)}$ is the total error of the jth external cable under the ith error condition, $\delta^a_{l(i,j)}$ is the length error of the jth active surface cable under the ith error condition (j = 1, 2. . ., n), and $\delta^a_{c(i,j)}$ is the coordinate error of the jth active surface cable node under the ith error condition (j = 1, 2. . ., n).

The error matrix of the giant cable-net structure can be expressed as

$$\Delta_{(i)} = \begin{pmatrix} \Delta^{OP}_{LC(i)} & 0 \\ \Delta^{IP}_{L(i)} & 0 \\ \Delta^{A}_{LC(i)} & \Delta^{A}_{T(i)} \end{pmatrix} = \begin{pmatrix} \Delta^{OP}_{L(i)} + \Delta^{OP}_{C(i)} & 0 \\ \Delta^{IP}_{L(i)} & 0 \\ \Delta^{A}_{L(i)} + \Delta^{A}_{C(i)} & \Delta^{A}_{T(i)} \end{pmatrix} = \begin{pmatrix} \delta^{op}_{l(i,1)} + \delta^{op}_{c(i,1)} & 0 \\ \delta^{op}_{l(i,2)} + \delta^{op}_{c(i,2)} & 0 \\ \vdots & \vdots \\ \delta^{op}_{l(i,k)} + \delta^{op}_{c(i,k)} & 0 \\ \delta^{ip}_{l(i,1)} & 0 \\ \delta^{ip}_{l(i,2)} & 0 \\ \vdots & \vdots \\ \delta^{ip}_{l(i,m)} & 0 \\ \delta^{a}_{l(i,1)} + \delta^{a}_{c(i,1)} & \delta^{a}_{t(i,1)} \\ \delta^{a}_{l(i,2)} + \delta^{a}_{c(i,2)} & \delta^{a}_{t(i,2)} \\ \vdots & \vdots \\ \delta^{a}_{l(i,n)} + \delta^{a}_{c(i,n)} & \delta^{a}_{t(i,n)} \end{pmatrix} \tag{6}$$

where $\Delta_{(i)}$ is the error matrix of the *i*th error condition of the structure; $\Delta^{OP}_{LC(i)}$ is the total cable length error of the outline passive surface cables; $\Delta^{IP}_{L(i)}$ is the length error of the inline passive surface cables; $\Delta^{A}_{LC(i)}$ is the total cable length error of the active surface cables; $\Delta^{A}_{T(i)}$ is the tensioning force error of the active surface cables; $\Delta^{OP}_{L(i)}$ is the length error of the outline passive cables; $\Delta^{OP}_{C(i)}$ is the coordinate error of the outline passive cable nodes; $\Delta^{A}_{L(i)}$ is the length error of the active surface cables; $\Delta^{A}_{C(i)}$ is the coordinate error of the active surface cable nodes; $\delta^{op}_{l(i,j)}$ is the length error of the *j*th passive surface cable under the *i*th error condition (*j* = 1, 2. . ., *k*); $\delta^{op}_{c(i,j)}$ is the coordinate error of the *j*th passive surface cable node under the *i*th error condition (*j* = 1, 2. . ., *k*); $\delta^{ip}_{l(i,j)}$ is the length error of the *j*th inline passive surface cable under the *i*th error condition (*j* = 1, 2. . ., *m*); $\delta^{a}_{t(i,j)}$ is the tensioning force error of the *j*th active surface cable under the *i*th error condition (*j* = 1, 2. . ., *n*); *k* is the number of outline passive surface cables, which is 150; *m* is the number of inline passive surface cables, which is 6520; and *n* is the number of active surface cables, which is 150.

Generally, in single-error computing with only a cable length error, the cable force is affected by $\Delta^{OP}_{LC(i)}$, $\Delta^{IP}_{L(i)}$, and $\Delta^{A}_{LC(i)}$. However, in the composite error computing with a cable length error and cable force error, the force (including error) of the active surface cable is $(1 + \Delta T)T_0$, and thus, the effects of $\Delta^{OP}_{LC(i)}$, $\Delta^{IP}_{L(i)}$, and $\Delta^{A}_{LC(i)}$ can be ignored. In this case, the small elastic modulus method [43] can be used for the iteration operation of the second error computing case, as listed in the following steps:

① Multiply the elastic modulus of the active surface cable by a small reduction factor, η.

$$E^{a}_{(j)} = \eta \cdot E^{a}_{0(j)} \quad j = 1, 2, \cdots, n \tag{7}$$

② Determine the initial strain of the active surface cable according to the tensioning force $t^{a}_{(i,j)}$ input by external loading equipment, e.g., the lifting jack.

$$\varepsilon^{a}_{(i,j)} = t^{a}_{(i,j)} / \left(\eta E^{a}_{0(j)} A^{a}_{0(j)} \right) \quad j = 1, 2, \cdots, n \tag{8}$$

③ Obtain the cable force of the active surface cable under the force equilibrium state.

$$f^{a}_{(i,j)} = t^{a}_{(i,j)} + \Delta f^{a}_{(i,j)} = t^{a}_{(i,j)} + \eta E^{a}_{0(j)} A^{a}_{0(j)} \Delta l^{a}_{(i,j)} / l^{a}_{(j)} \quad j = 1, 2, \cdots, n \tag{9}$$

where η is the reduction coefficient of the elastic modulus; $E^{a}_{0(j)}$, $A^{a}_{0(j)}$, and $l^{a}_{(j)}$ are the designed elastic modulus, cross-sectional area, and cable length of the *j*th active surface cable, respectively; $E^{a}_{(j)}$ is the elastic modulus of the *j*th active surface cable multiplied by the reduction coefficient; $\varepsilon^{a}_{(i,j)}$ is the initial strain of the *j*th active surface cable under the *i*th error condition; $t^{a}_{(i,j)}$ and $\Delta l^{a}_{(i,j)}$ are the tensioning force and length increment of the *j*th active surface cable under the *i*th error condition, respectively; and $f^{a}_{(i,j)}$ and $\Delta f^{a}_{(i,j)}$ are the tensioning force and force increment of the *j*th active surface cable under the *i*th error condition, respectively.

If $\eta \approx 0$, then $\Delta f^{a}_{(i,j)} \approx 0$ and $f^{a}_{(i,j)} \approx t^{a}_{(i,j)}$, and the value of $\varepsilon^{a}_{(i,j)}$ is tremendously enlarged, which leads to a large expansion amount for the cables. On this basis, the iterative operation of the computing will converge to the static equilibrium state with a smaller number of iterations, and the final static equilibrium state of the overall structural model will be found efficiently. Therefore, if η is small enough, the tensioning force of the active surface cable can be easily changed, and the model analysis efficiency can be improved. In this study, η is defined as 0.001.

After finding the final static equilibrium state, the structural model is updated, the elastic modulus of the active surface cables is recovered, and the strains on the active surface cables are multiplied by η to maintain the cable forces.

3. Establishment of the Giant Cable-Net Model

The complete ANSYS model of the giant cable-net structure, including cables, beams, and columns, is shown in Figure 6. According to Figure 6, the FAST reflector was designed as a 500 m diameter spherical cable net woven by the short-range line-type meshing method. The complete model is established based on the modeling theory of short-range line-type shells and the APDL parametric language. The detailed modelling principle is the same as Zheng et al. [44], and the control method for cables follows Zhao et al. [45].

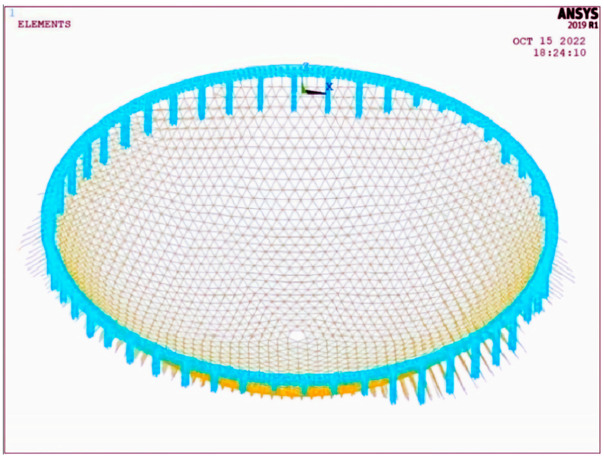

Figure 6. Complete ANSYS model of the giant cable-net structure.

In this model, the BEAM 44 element is used to simulate the steel ring truss and pillar components due to its ability to withstand tension, compression, torsion, and bending. The LINK 180 element is used to simulate all the cables in the model due to its ability to withstand tension or compression in the direction of the rod axis. Because the cables are not compressed, they are set to be tension-only. While the requirements for the speed of analysis are significant, each segment of cable between the adjacent nodes is meshed into one element. The weight of the reflector panel is transformed to vertical loads at the intersections of the pull-down cables and main cables. The specific unit types are shown in Figure 7. The parameters of the cable body, cable head, and crossing nodes are listed in Table 2.

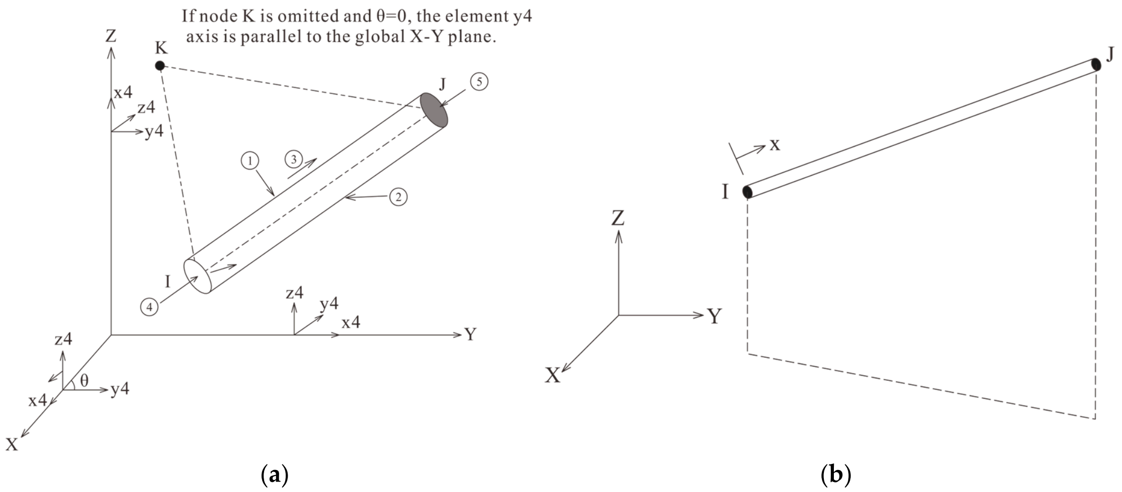

(**a**) (**b**)

Figure 7. Element types in the numerical model. (**a**) Three-dimensional two-node beam element (BEAM44); (**b**) three-dimensional two-node cable element (LINK180).

Table 2. Parameters of the cable body, cable head, and crossing nodes.

No.	Specification	Cable Body				Cable Head		Crossing Node
		Area (cm^2)	Linear Weight (kg/m)	Outside Diameter (mm)	Ultimate Bearing Force (kN)	Mass (kg)	Length (mm)	Mass (kg)
1	OVM.ST15-1	1.4	1.37	23	260	10.5	390	41
2	OVM.ST15-2	2.8	3.29	44	520	40	640	41
3	OVM.ST15-2J3	3.4	3.65	44	629.5	40	640	41
4	OVM.ST15-3	4.2	4.52	47	782	52	700	55
5	OVM.ST15-3J3	4.8	4.87	47	891.5	52	700	55
6	OVM.ST15-4	5.6	5.71	51	1040	70	800	90
7	OVM.ST15-4J3	6.2	6.07	51	1149.5	70	800	90
8	OVM.ST15-5	7	7.29	62	1300	87	830	115
9	OVM.ST15-5J3	7.6	7.75	62	1409.5	87	830	115
10	OVM.ST15-6	8.4	8.29	62	1560	92	880	132
11	OVM.ST15-6J3	9	8.75	62	1669.5	92	880	132
12	OVM.ST15-7	9.8	9.29	62	1820	108	880	172
13	OVM.ST15-7J3	10.4	9.75	62	1929.5	108	880	172
14	OVM.ST15-8	11.2	11.22	74	2080	151	1020	194
15	OVM.ST15-8J3	11.8	11.68	74	2189.5	151	1020	194
16	OVM.ST15-9	12.6	12.52	80	2340	185	1030	253
17	OVM.ST15-9J3	13.2	12.99	80	2449.5	185	1030	253
18	OVM.ST15-10	14	13.52	80	2600	199	1120	268
19	OVM.ST15-10J3	14.6	13.99	80	2709.5	199	1120	268
20	OVM.ST15-11	15.4	14.74	81	2860	212	1150	307
21	OVM.ST15-11J3	16	15.2	81	2969.5	212	1150	307

4. Error Combination Computing

The length error of the surface cable is Δ_{1L}, the length error of the control cable is Δ_{2L}, the installation error of the external node is Δ_C, and the tensioning force error ratio of the active surface cable is Δ_T.

The specific steps of error combination computing are shown as follows:

(1) The error distribution models of Δ_{1L}, Δ_{2L}, Δ_C, and Δ_T are determined by a normal distribution.

(2) According to the statistical data-based Monte Carlo method [40], a sufficient number of error samples are generated in which each error sample is an error condition of the structure. Figure 8 shows the distribution of 1000 error samples randomly generated by one of the control cables. Set the range of control cable error to [−15 mm, 15 mm], the average value to 0 mm, and the variance to 25. The maximum value of the actual sample is 14.91 mm, the minimum value is −15 mm, the average value is −0.055 mm, and the variance is 27.03, which follows a normal distribution.

(3) Introduce each error sample into the cable net to form the defective structure condition.

(4) Obtain the error influence of the cable net under each working condition.

(5) Compare the stresses of cables under the conditions of defective and ideal working conditions and count the maximum cable stress error.

(6) Judge whether the maximum cable stress error meets the requirements. According to the provisions of Technical Specification for Prestressed Steel Structures [46], the maximum error is taken to be ±10%. If it meets the requirements, this indicates that the allowable range of error parameters is set reasonably. Otherwise, the allowable range of error parameters is adjusted, and steps (1) through (5) are repeated until a reasonable allowable range of error parameters is obtained.

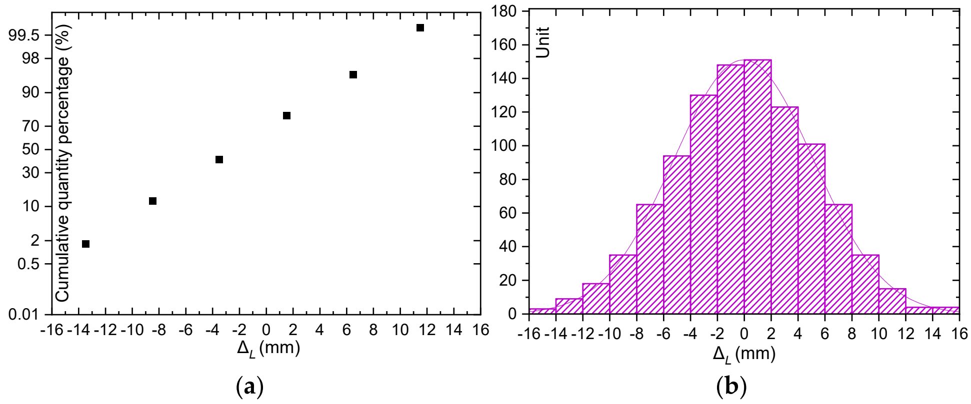

Figure 8. Distribution of 1000 error samples generated by a control cable: (**a**) cumulative percentage of errors; (**b**) number of errors.

Considering that the manufacturing process of the FAST cable-net structure has strict quality control [47], the error between the calibrated reference sphere of the cable net and the standard reference sphere should not exceed 2 mm, the allowable error limit for the cable force is ± 10%, and the maximum displacement of the cable-net node is set to 20 mm. Thirteen error combinations are set in Table 3 on the premise that the cable-net structure is in a spherical reference state. A total of 1000 samples are randomly established for each error combination, and the distribution model is a normal distribution model.

Table 3. Error combinations.

Error Combination	Length Error of Passive Surface Cable Δ_{1L} (mm)	Length Error of Control Cable Δ_{2L} (mm)	External Cable	
			Installation Error Δ_C(mm)	Tensioning Force Error Ratio Δ_T (%)
1	≤1	—	—	—
2	≤1.5	—	—	—
3	—	≤10	—	—
4	—	≤15	—	—
5	—	≤20	—	—
6	—	—	≤2	—
7	—	—	≤3	—
8	—	—	≤4	—
9	—	—	—	≤5
10	—	—	—	≤10
11	≤1.5	≤20	—	—
12	≤1.5	≤20	—	≤5
13	≤1.5	≤20	—	≤10

First, single-error influence computing is carried out (error combinations 1~10) to determine the influence degree of each error on the structure. Then, multi-error coupling influence computing (error combination 11~13) is performed to determine the control index of each error. The error computing of the cable force adopts a 95% assurance rate, that is, twice the standard deviation.

5. Error Computing Results

5.1. Single-Error Influence Computing

When the cable-net structure is in the spherical reference state, the influence degrees of each independent error on the adjustment of the cable force and external cable length are shown in Table 4, in which the simulation results calculated by the method in Chen et al., 2018 [27] have also been displayed.

Table 4. Effect of independent errors.

Error Combination	Force Error Ratio of Passive Surface Cable (%)		Force Error Ratio of Control Cable (%)		External Cable			
					Force Error Ratio (%)		Required Adjustment of Cable Length (mm)	
	This Study	Chen et al., 2018 [27]	This Study	Chen et al., 2018 [27]	This Study	Chen et al., 2018 [27]	This Study	Chen et al., 2018 [27]
1	3.97	3.18	1.22	0.49	1.33	0.40	—	
2	5.96	2.38	1.84	0.37	1.99	0.40	—	
3	3.48	0.70	1.16	0.81	0.71	0.21	—	
4	2.22	1.55	4.23	1.27	1.06	0.64	—	
5	2.9	0.87	6.31	1.26	1.41	0.99	—	
6	2.90	0.58	1.72	0.52	2.00	1.40	—	
7	4.35	1.31	2.58	1.55	3.00	2.40	—	
8	5.80	3.48	3.43	2.40	4.00	0.80	—	
9	6.16	4.31	5.90	4.13	—		±23.4	±16.4
10	12.32	8.62	11.82	9.46	—		±46.9	±37.5

The results show that different kinds of errors lead to diverse force error ratios and various adjustments of external cable lengths. The tensioning force error ratio Δ_T makes the greatest impact on the variation of the simulation model. A 5% error ratio in tensioning force causes ±23.4 mm in required adjustment of the cable length, 6.16% in force error ratio of the passive surface cable, and 5.90% in force error ratio of the control cable. Moreover, a small change in the installation error of the external cables greatly affects the forces of all the cables, while a relatively larger length error of the control cable makes a nonsignificant impact. Comparing the results simulated by the method of this study and the theory proposed in Chen et al., 2018 [27], it is obvious that most error ratios for cables and required adjustment of cable lengths simulated by Chen et al., 2018 [27] are much less than the analyzed results of the error influence computing method. In this case, the proposed error influence computing method will, in some ways, amplify the effect of these error parameters and will bias the design towards safety.

Based on error combination 1, 60 cables with the largest force error ratio of surface cables and control cables are selected. The force error ratio of these cables is arranged from small to large, and the serial number of these cables is designed from l to 60. Then, we compare the force errors of these cables under error combinations 1 and 2, as shown in Figures 9 and 10.

By comparing the ratios of error values of any two cables in Figure 8 or Figure 9, the results show that with the increase in the length error of the surface cables, the tensioning force errors of the surface cable and control cable also increase, and the force error ratios of the surface cables, control cables, and external cables all have a linear relationship with the length error of the surface cables. For example, as displayed in Figure 8, the force error ratio of surface cable #1 is 2.245% and 3.368% under error combinations 1 and 2, respectively, and the ratio of these two values is 0.666. For surface cable #1, the force error ratio of surface cable #50 is 3.266% and 4.899% under error combinations 1 and 2, and the ratio of these two values is 0.667. The two ratios of surface cable #1 and surface cable #50 are very close.

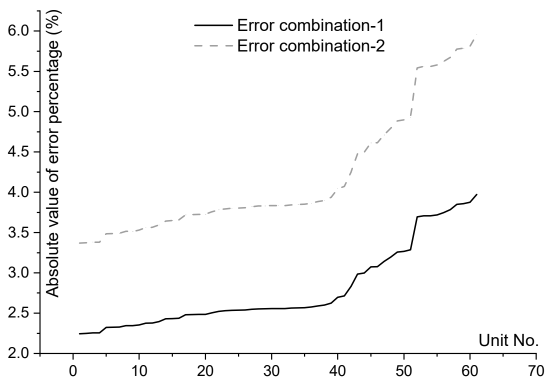

Figure 9. Force error ratio of the surface cable in error combinations 1 and 2.

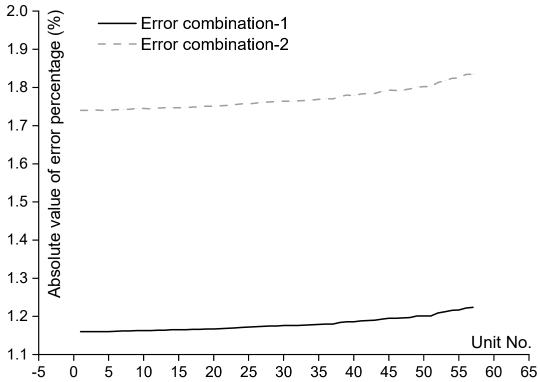

Figure 10. Force error ratio of the control cable in error combinations 1 and 2.

Therefore, an error influence degree coefficient, δ, can be defined as shown in Equation (10), that is, the maximum cable force error ratio caused by cable length error per unit length (or tensioning force error per unit percentage). The mathematical expression is

$$\delta = \frac{\Delta_F}{\Delta} \tag{10}$$

where ΔF is the maximum cable force error ratio and Δ is the error of the cable length or cable force error ratio.

Table 5 lists the influence degree coefficient of each error combination calculated by Equation (10). The length error of the surface cable has the greatest influence on the force error of passive surface cables, control cables, and external cables and thus is an error influence factor. The influences of the installation error of the external nodes and the tensioning force error ratio of the active surface cables are slightly smaller, and thus, these two errors are also sensitive factors. The cable length error of the control cable has the least influence and thus is an insensitive factor.

Table 5. Error influence degree coefficient δ.

Error Type	Force Error of Passive Surface Cable	Force Error of Control Cable	Tensioning Force Error of External Cable
Length error of surface cable (%/mm)	3.97	1.23	1.33
Length error of control cable (%/mm)	0.15	0.62	0.07
Installation error of external node (%/mm)	1.45	0.86	1.00
Tensioning force error ratio of external cable (%/%)	1.23	1.18	—

5.2. Multi-Error Coupling Influence Computing

Because the lengths of the active surface cables are adjustable, the tensioning force error of the active surface cables, the length error of the passive surface cables, and the length error of the control cables are considered in the multi-error coupling influence computing, while the coordinate error of the external nodes is not taken into account.

Based on error combination 13, 45 surface cables and control cables with the largest force error ratios are selected and arranged in order from small to large ratios. The unit number is set from 1 to 45. Then, the force error ratios of these cables under error combinations 11 to 13 are compared, as shown in Figures 11 and 12. The results of the force error ratios of the passive surface cable, control cable, and external cable are given in Table 6, with the required adjustment of cable length.

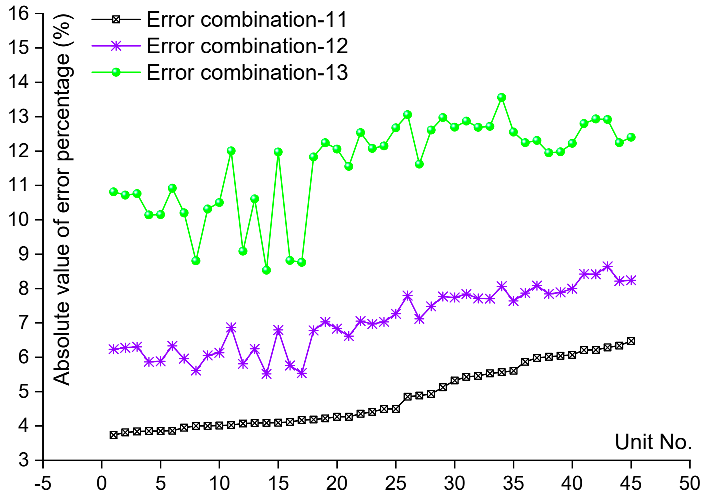

Figure 11. Force error ratios of surface cables in error combinations 11, 12, and 13.

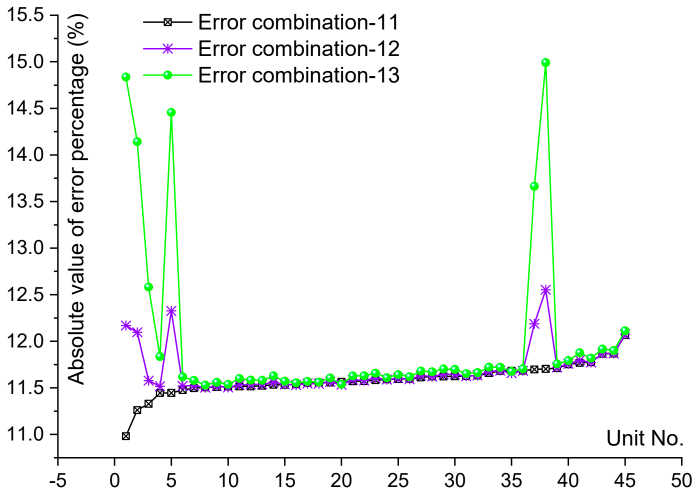

Figure 12. Force error ratios of control cables in error combinations 11, 12, and 13.

Table 6. Influence of multi-error coupling combinations.

Error Combination	Force Error Ratio of Passive Surface Cable (%)		Force Error Ratio of Control Cable (%)		External Cable			
					Force Error Ratio (%)		Required Adjustment of Cable Length (mm)	
	This Study	Chen et al., 2018 [27]	This Study	Chen et al., 2018 [27]	This Study	Chen et al., 2018 [27]	This Study	Chen et al., 2018 [27]
11	6.48	4.86	12.07	9.66	2.31	1.39	—	
12	8.64	5.18	12.56	7.54	—		±23.7	±20.7
13	13.56	9.49	14.99	10.49	—		±47.4	±39.1

From a comparison of the results in Tables 4 and 6, it is obvious that when the length error limits of the surface cable and control cable are set to ±1.5 mm and ±20 mm, respectively, the force error ratios of the passive surface cable and control cable present a positive correlation with the force error ratio of the active surface cable. In this case, the force error ratio of active surface cables has an adverse impact on the forces of most surface cables and a small number of control cables, and this influence basically presents a linear relationship. In addition, the coupling effect of multiple errors is not a linear superposition of each error's influence and is somewhat less than that. When the tensioning force error limit of the active surface cables is set to ±10%, the length adjustment required for the active surface cables is smaller than ±47.4 mm, while the cable length adjustment in actual projects is generally larger than ±90 mm, as obtained from the product instructions. In this case, the tensioning force error limit of the active surface cables and the installation error limit of the external node for the giant cable-net structure in this project can be set to ±10% and ±50 mm, respectively.

6. Discussion

This research introduces an error sensitivity computing method based on a normal distribution to perform single-error computing and multi-error coupling computing of the giant cable net of a Chinese 500 m aperture spherical radio telescope. The results indicate that this method gives the procedure limits and installation limits of surface cables, control cables, and external nodes of surrounding supporting structures, which provides a basis for the actual construction control of the 500 m giant cable-net structure. The advantages and future validation of the methods, as well as the additional socioenvironmental implications, limitations, adaptability, and reproducibility, are further discussed below.

6.1. Advantages and Innovations of the Methods

This paper mainly discusses the error influence of the lengths of the surface cables and control cables, the tensioning forces of active surface cables, and the installation coordinates of external nodes on the 500 m giant cable-net structure. This is an important case study focusing on error sensitivity computing for cable-supported structures, setting a valuable example for the field of construction control of large-span structures.

This methodology is practical and helpful for the key beneficiary (e.g., the design institute and the manufacturer) to make decisions about the length error limits, force error limits, and installation error limits of the cables and nodes. The computing method is specifically designed to find the relationships between different error parameters and to distinguish the importance of each influencing factor. Therefore, it can determine a reasonable construction accuracy control index.

Furthermore, the proposed computing process, as well as the results, can be extended to similar long-span cable-supported structures to reduce the influence of error on structural performance.

6.2. Limitations

Similar to any other error computing theory, the error sensitivity computing method proposed in this study is not perfect. The results reported in this section have certain limitations, summarized as follows:

1. The usability of the error sensitivity computing method, currently based on the 500 m giant cable-net structure, needs to be tested and validated in further work to expand its applicability.
2. According to Jin et al. [30], the error of cable cross-sectional areas is also an important parameter that affects the constructional forming forces of cables. In this study, the error influence computing is conducted on the premise that the cross-sectional areas of all the cables are known in advance, which is suitable for the 500 m giant cable-net structure based on the relatively more important requirements for structural mechanical performance, but this assumption may not be fully applicable to all situations.
3. Several published studies [48,49] have stated the influence of the outer compressive ring beam (boundary) on the internal forces of cable nets. In this study, this part is implemented by analyzing the installation coordinates of external nodes on the outer compressive ring after tensioning the cables, while the stiffness of the outer ring beam is not considered, which may cause minor second-order deformations to change the forces of the cables.

6.3. Adaptability and Reproducibility

As shown in the previous sections, this case study provides a simple but useful example of a way to find the main and secondary error factors affecting the cable forces of a 500 m cable-net structure as well as the limits of these errors, which gives an important example for the construction control of large-span cable-net structures. The demonstrated processes of single-error computing and multi-error coupling computing are highly adaptable and reproducible. Therefore, researchers, engineers, designers, and policy makers can easily follow and customize this method to determine a detailed construction control index for similar long-span cable-supported structures.

7. Conclusions

(1) When conducting single-error influence computing, the length error of surface cables has the greatest influence on the force errors of passive surface cables, control cables, and external cables and is a sensitive factor. The tensioning force error of the active surface cables and the installation error of the external nodes have slightly smaller effects, and thus, these two errors are also sensitive factors. The length error of the control cables has the least influence on the force error of all the cables and thus is an insensitive factor.

(2) When performing multi-error coupling influence computing, the coupling effect of multiple errors is not the linear superposition of independent error influences but has a certain reduction for the superposition value. Therefore, the main error factors should be comprehensively considered for coupling computing to reasonably determine the control index of each error.

(3) Through multi-error coupling computing, the main error control index of the giant cable-net structure is determined: the length error limits of the surface cable and control cable are $\pm$ 1.5 mm and $\pm$ 20 mm, respectively; the tension error limit of the active surface cable is $\pm$ 10%; and the installation error limit of the external node is $\pm$ 50 mm.

(4) As a natural extension of this research, while this manuscript provides valuable insights into the error influence simulation of an enormous cable-net structure based on random combinations, it would be beneficial to include suggestions for future research directions. The error sensitivity computing method proposed in this study will be utilized to analyze other types of cable-strut structures, such as the cable dome, the cable truss, the suspen-dome, etc.

Author Contributions: Conceptualization, L.W. and M.D.; Data curation, Y.R. and J.G.; Formal analysis, M.D.; Funding acquisition, B.L.; Investigation, L.W. and Y.R.; Methodology, J.G.; Project administration, L.W.; Resources, B.L.; Software, L.W.; Supervision, B.L.; Validation, M.D.; Visualization, Y.R.; Writing—original draft, L.W. and M.D.; Writing—review & editing, M.D. All authors have read and agreed to the published version of the manuscript.

Funding: This research was funded by the National Natural Science Foundation of China, grant number 11673039; the Natural Science Foundation of Jiangsu Province, grant number BK20190753; the Natural Science Foundation of the Jiangsu Higher Education Institutions of China, grant number 18KJB560011; and the Priority Academic Program Development of Jiangsu Higher Education Institutions (PAPD). The APC was funded by the Natural Science Foundation of Jiangsu Province, grant number BK20190753.

Institutional Review Board Statement: Not applicable.

Informed Consent Statement: Not applicable.

Data Availability Statement: The data presented in this study are available on request from the corresponding author.

Conflicts of Interest: The authors declare no conflict of interest.

References

1. Dong, F.H.; Zhang, H.H. Probabilistic Safety Factor Calculation of the Lateral Overturning Stability of a Single-Column Pier Curved Bridge under Asymmetric Eccentric Load. *Symmetry* **2022**, *14*, 1534. [CrossRef]
2. Duan, M.J.; Suo, X.C.; Dong, F.H.; Li, J.H.; Li, G.F. Research on the Control Method for the Reasonable State of Self-Anchored Symmetry Suspension Bridge Stiffening Girders. *Symmetry* **2022**, *14*, 935. [CrossRef]
3. Li, Q.W.; Jiang, P.; Li, H. Prognostics and health management of FAST cable-net structure based on digital twin technology. *Res. Astron. Astrophys.* **2020**, *20*, 49–56. [CrossRef]
4. Yu, Y.Z.; Peng, B.; Liu, K.; Zhang, C.M.; Wang, L.; Kou, F.F.; Lu, J.G.; Yu, M. FAST Ultrawideband Observation of Abnormal Emission-shift Events of PSR B0919+06. *Sci. China Phys. Mech. Astron.* **2019**, *62*, 95904. [CrossRef]
5. Lu, J.G.; Peng, B.; Xu, R.X.; Yu, M.; Dai, S.; Zhu, W.W.; Yu, Y.Z.; Jiang, P.; Yue, Y.L.; Wang, L. The Radiation Structure of PSR B2016+28 observed with FAST. *Sci. China Phys. Mech. Astron.* **2019**, *62*, 959505. [CrossRef]
6. Lu, J.G.; Peng, B.; Liu, K.; Jiang, P.; Yue, Y.L.; Yu, M.; Yu, Y.Z.; Kou, F.F.; Wang, L. Study of Three Rotating Radio Transients with FAST. *Sci. China Phys. Mech. Astron.* **2019**, *62*, 959503. [CrossRef]
7. Luo, B.; Ding, M.M.; Xie, G.R.; Guo, Z.X. Accumulative Traction Construction Analysis of the FAST Cable-net Structure. *KSCE J. Civ. Eng.* **2018**, *22*, 3707–3717. [CrossRef]
8. Li, D.; Pan, Z. The Five-hundred-meter Aperture Spherical Radio Telescope project. *Radio Sci.* **2016**, *51*, 1060–1064. [CrossRef]
9. Li, G.Q.; Shen, L.Y.; Luo, Y.F.; Deng, C.G.; He, Y.M. Analysis for Reflector Aluminum Mesh Panels of Five-Hundred Meter Aperture Spherical Telescope. *Astrophys. Space Sci.* **2001**, *278*, 225–230. [CrossRef]
10. Jiang, P.; Yue, Y.L.; Gan, H.Q.; Yao, R.; Li, H.; Pan, G.F.; Sun, J.H.; Yu, D.J.; Liu, H.F.; Tang, N.Y.; et al. Commissioning Progress of the FAST. *Sci. China Phys. Mech. Astron.* **2019**, *62*, 959502. [CrossRef]
11. Zhu, W.X.; Jia, K.F.; Fu, F.; Lan, D.Q.; Qian, K. A new design of cable anchor for ultrahigh fatigue stress cable net of largest telescope in the world. *Thin-Walled Struct.* **2021**, *159*, 107280. [CrossRef]
12. Zhang, Y.; Wei, Y.; Bing, L.; Wang, G.; Huang, L. A novel seawater and sea sand concrete-filled FRP-carbon steel composite tube column: Seismic behavior and Finite-Element Analysis. *Eng. Struct.* **2022**, *270*, 114872. [CrossRef]
13. Wei, Y.; Zhu, C.; Miao, K.; Chai, J.; Zheng, K. Compressive behavior of rectangular concrete-filled fiber-reinforced polymer and steel composite tube columns with stress-release grooves. *Compos. Struct.* **2022**, *281*, 114984. [CrossRef]
14. Chen, S.; Wei, Y.; Ding, M.; Zhao, K.; Zheng, K. Combinatorial design and flexural behavior of laminated bamboo-timber composite beams. *Thin-Walled Struct.* **2022**, *181*, 109993. [CrossRef]
15. Zhao, L.; Cao, Z.; Wang, Z.; Fan, F. Initial prestress design and optimization of cable-stiffened latticed shells. *J. Constr. Steel Res.* **2021**, *184*, 106759. [CrossRef]
16. Wan, Z.; Cao, Z.; Sun, Y.; Fan, F. Experimental and numerical research on the structural behaviour of a Tensairity dome. *Eng. Struct.* **2021**, *248*, 113225. [CrossRef]
17. Liu, F.; Wang, L.; Jin, D.; Wen, H. Equivalent continuum modeling of beam-like truss structures with flexible joints. *Acta Mech. Sinica* **2019**, *35*, 1067–1078. [CrossRef]
18. Liu, F.; Wang, L.; Jin, D.; Liu, X.; Lu, P. Equivalent micropolar beam model for spatial vibration analysis of planar repetitive truss structure with flexible joints. *Int. J. Mech. Sci.* **2020**, *165*, 105202. [CrossRef]
19. Bäck, J.; Nobile, F.; Tamellini, L.; Tempone, R. Stochastic spectral Galerkin and collocation methods for PDEs with random coefficients: A numerical comparison. In *Spectral and High Order Methods for Partial Differential Equations*; Springer: Berlin/Heidelberg, Germany, 2011; pp. 43–62.
20. Nobile, F.; Tempone, R.; Webster, C.G. A sparse grid stochastic collocation method for partial differential equations with random input data. *SIAM J. Numer. Anal.* **2008**, *46*, 2309–2345. [CrossRef]
21. Bonizzoni, F.; Nobile, F. Regularity and sparse approximation of the recursive first moment equations for the lognormal Darcy problem. *Comput. Math. Appl.* **2020**, *80*, 2925–2947. [CrossRef]
22. Bonizzoni, F.; Nobile, F.; Kressner, D. Tensor train approximation of moment equations for elliptic equations with lognormal coefficient. *Comput. Method. Appl. Mech. Eng.* **2016**, *308*, 349–376. [CrossRef]
23. Chen, L.M.; Deng, H.; Ye, X.G.; Dong, S.L.; Zhou, Y.Y. Theoretical analysis and experimental research on element-length error sensitivity of cable-bar tensile structures. *J. Build. Struct.* **2015**, *36*, 93–100. (In Chinese)
24. Zong, Y.L.; Hu, N.G.; Duan, B.Y.; Yang, G.G.; Cao, H.J.; Xu, W.Y. Manufacturing error sensitivity analysis and optimal design method of cable-network antenna structures. *Acta Astronaut.* **2016**, *120*, 182–191. [CrossRef]
25. Luo, B.; Sun, Y.; Guo, Z.X.; Pan, H.T. Multiple random-error effect analysis of cable length and tension of cable–strut tensile structure. Adv. *Struct. Eng.* **2016**, *19*, 1289–1301. [CrossRef]
26. Chen, L.; Hu, D.; Deng, H.; Cui, Y.; Zhou, Y. Optimization of the construction scheme of the cable-strut tensile structure based on error sensitivity analysis. *Steel Compos. Struct.* **2016**, *21*, 1031–1043. [CrossRef]
27. Chen, L.M.; Gao, W.F.; Hu, D.; Zhou, Y.Y.; Zhang, F.B.; Dong, S.L. Determination of a Monitoring Scheme for Controlling Construction Errors of a Cable-strut Tensile Structure. *KSCE J. Civ. Eng.* **2018**, *22*, 4030–4037. [CrossRef]
28. Yang, Y. Optimal topology design of replaceable bar dampers of a reticulated shell based on sensitivity analysis. *Earthq. Eng. Eng. Vib.* **2014**, *1*, 113–124. [CrossRef]
29. Sun, Z.H.; Duan, B.Y.; Zhang, Y.Q.; Yang, D.W. Influence and experiment of cable-net manufacturing errors on surface accuracy of mesh reflector antennas. *Chin. J. Aeronaut.* **2023**, *36*, 363–376. [CrossRef]

30. Jin, X.F.; Fan, F.; Shen, S.Z. Parameter sensitivity analysis of the cable-net structure supporting the reflector of a large radio telescope-FAST. *Tumu Gongcheng Xuebao/China Civ. Eng. J.* **2010**, *2*, 12–19. (In Chinese)
31. Xu, K.; Peng, J.; Wang, Q.M. A Study of Influences of Value Variations of Structural Parameters on Forces in Cables in the Net Structure of Cables of the FAST. *Astron. Res. Technol.* **2015**, *2*, 159–165. (In Chinese)
32. Yang, C.; Xia, Y. Interval Uncertainty-oriented Optimal Control Method for Spacecraft Attitude Control. *IEEE Trans. Aerosp. Electron. Syst.* **2023**, *59*, 5460–5471. [CrossRef]
33. Yang, C.; Lu, W.; Xia, Y. Uncertain optimal attitude control for space power satellite based on interval Riccati equation with non-probabilistic time-dependent reliability. *Aerosp. Sci. Technol.* **2023**, *139*, 108406. [CrossRef]
34. Yang, C.; Lu, W.; Xia, Y. Reliability-constrained optimal attitude-vibration control for rigid-flexible coupling satellite using interval dimension-wise analysis. *Reliab. Eng. Syst. Safe.* **2023**, *237*, 109382. [CrossRef]
35. Yang, C.; Yu, Q. Placement and size-oriented heat dissipation optimization for antenna module in space solar power satellite based on interval dimension-wise method. *Aerosp. Sci. Technol.* **2023**, *134*, 108155. [CrossRef]
36. Yang, C. An adaptive sensor placement algorithm for structural health monitoring based on multi-objective iterative optimization using weight factor updating. *Mech. Syst. Signal Process.* **2021**, *151*, 107363. [CrossRef]
37. Yang, C.; Ouyang, H. A novel load-dependent sensor placement method for model updating based on time-dependent reliability optimization considering multi-source uncertainties. *Mech. Syst. Signal Process.* **2022**, *165*, 108386. [CrossRef]
38. Yang, C.; Xia, Y. A novel two-step strategy of non-probabilistic multi-objective optimization for load-dependent sensor placement with interval uncertainties. *Mech. Syst. Signal Process.* **2022**, *176*, 109173. [CrossRef]
39. Shen, Y.; Luo, B.; Jiang, P.; Ding, M.; Li, Q.; Wei, Y. Development of a Pre-Evaluation and Health Monitoring System for FAST Cable-Net Structure. *Appl. Sci.* **2022**, *12*, 332. [CrossRef]
40. Betancur, D.; Duarte, L.F.; Revollo, J.; Restrepo, C.; Díez, A.E.; Isaac, I.A.; López, G.J.; González, J.W. Methodology to Evaluate the Impact of Electric Vehicles on Electrical Networks Using Monte Carlo. *Energies* **2021**, *14*, 1300. [CrossRef]
41. *JGJ 257-2012, J1402—2012*; Technical Specification for Cable Structures. China Architecture & Building Press: Beijing, China, 2012. (In Chinese)
42. *ASCE/SEI STANDARD 19-10*; Structural Applications of Steel Cables for Buildings. The American Society of Civil Engineers: Reston, VA, USA, 2010.
43. Gao, Q.Y.; Zhang, Q.B.; Tang, Q.G.; Feng, Z.W. Form optimization design of space net using small elastic modulus method. *J. Natl. Univ. Def. Technol.* **2017**, *39*, 1–5. [CrossRef]
44. Zheng, X.L.; Xiong, J.M.; Zhou, J.Z. Application of APDL Parametric Language in FAST Main Cable Network Structure Modeling. *J. Hubei Univ. Technol.* **2018**, *33*, 112–114. [CrossRef]
45. Zhao, Y.; Guo, J.; Jiang, Z.; Chen, W.; Zhou, G. Control method for determining feasible prestresses of cable-struts structure. *Thin-Walled Struct.* **2022**, *174*, 109159. [CrossRef]
46. *CECS 212: 2006*; Technical Specification for Prestressed Steel Structures. The Chinese Overseas Publishing House: Beijing, China, 2006. (In Chinese)
47. Xie, G. *Research on the Key Technology of Accumulative Sliding along Guide-Rope of Serial Cables at High Altitude of FAST*; Southeast University: Nanjing, China, 2015.
48. Asghari, R.; Abedi, K.; Chenaghlou, M.R. Investigation into pre-stress modes and optimal layout of a new hybrid cable-strut system. *Adv. Struct. Eng.* **2020**, *23*, 1259–1275. [CrossRef]
49. Diaz, J.J.D.C.; Nieto, P.J.G.; Fresno, D.C.; Fernández, E.B. Non-linear analysis of cable networks by FEM and experimental validation. *Int. J. Comput. Math.* **2009**, *86*, 301–313. [CrossRef]